Transactions of the Materials Research Society of Japan 31[1] 73-76 (2006)

Effect of Oxygen Radical Irradiation of $Bi_4Ti_3O_{12}$ Thin Films by Two-Dimensional RF Magnetron Sputtering

Naoko Inada, Tohru Higuchi, Hiroaki Masaya, Hironobu Ogawa, Mayumi Iwasa, Takeshi Hattori and Takeyo Tsukamoto
Department of Applied Physics, Tokyo University of Science, 1-3 Kagurazaka, Shinjuku, Tokyo 162-8601, Japan
Fax: 81-3-5228-8241, e-mail: higuchi@rs.kagu.tus.ac.jp

The $Bi_4Ti_3O_{12}$ (BIT) thin films were prepared on $Pt/Ti/SiO_2/Si$ substrates by two-dimensional RF magnetron sputtering using TiO_2 and Bi_2O_3 targets. In order to achieve low temperature crystallization, we tried to irradiate the oxygen radical with high reactive during the deposition. The oxygen radical irradiated BIT thin film exhibited *a*- and *b*-axes orientation, although the non-irradiated BIT thin film exhibited highly *c*-axis orientation. The prepared BIT thin film consisted of small grains with diameters of around ~50 nm. The BIT thin film exhibited the ferroelectricity without postannealing. These findings are unique phenomenon of oxygen radical irradiation for BIT thin film deposition.

Key words: $Bi_4Ti_3O_{12}$ (BIT), thin film, RF magnetron sputtering, oxygen radical, orientation

1. INTRODUCTION

Ferroelectric $Bi_4Ti_3O_{12}$ (BIT) films are expected for application to nonvolatile ferroelectric memory (NV-FeRAM) devices with nondestructive readout operation. The BIT thin film with Pt electrode is considered a promising due to its excellent fatigue endurance. However, it is difficult to prepare a perfect BIT thin film since interdiffusion occurs between the electrode and poly-Si plug during ferroelectric film formation at high crystallization temperatures [1-5]. Therefore, the formation process at low temperatures below 500°C is desirable for the realization of poly-Si-plug stacked capacitor memory cells.

In recent years, preparation of BIT thin film has been investigated by several deposition techniques such as sol-gel [4,5], metalorganic decomposition (MOD) [6,7], metalorganic chemical vapor deposition (MOCVD) [8-14], and RF magnetron sputtering [15-21]. From the point of view of commercial production using sol-gel, MOD, and MOCVD methods, there are still some severe difficulties, for instance poor throughput (low deposition rate), high-temperature deposition, compositional nonuniformity across large substrate, rough surface morphology, lack of appropriate precursors in the gas phase, and poor reproducibility. In order to resolve these problems, the authors have prepared the BIT thin films on $Pt/Ti/SiO_2/Si$ substrate by two-dimension RF magnetron sputtering [17,21]. When the RF powers of Bi_2O_3 and TiO_2 were fixed at 100 W and 200 W, respectively, the BIT film exhibited the *c*-axis orientation. Although the prepared BIT thin film consisted of well-developed grains, the good ferroelectricity was not observed due to interdiffusion with high postannealing temperatures.

In this study, we have prepared the BIT thin films on $Pt/Ti/SiO_2/Si$ substrates by oxygen-radical assist-type two-dimensional RF magnetron sputtering using Bi_2O_3 and TiO_2 targets. The oxygen radical has high reactive more than O_2 gas, since the oxygen radical has an unstable unpaired electron. In order to achieve low temperature crystallization, the oxygen radical with high reactive was irradiated during the deposition of BIT thin film. In this paper, we present the effect of oxygen radical irradiation for BIT thin films deposition.

2. EXPERIMENTAL

BIT thin films were deposited by RF magnetron reactive sputtering using TiO_2 and Bi_2O_3 ceramic multitargets. The TiO_2 and Bi_2O_3 ceramic targets were prepared as follows [18]. The TiO_2 (99.99 %) powder was pressed into disk (5 inch in diameter). The pressed TiO_2 disk was sintered at 1250°C for 6 hours. The Bi_2O_3 (99.9 %) powder was pressed into disk (5 inch in diameter). The pressed Bi_2O_3 disk was sintered at 750°C for 6 hours. The thickness of Bi_2O_3 and TiO_2 targets was fixed at 4.55 mm and 3.20 mm, respectively. These ceramic targets were examined using XRD analysis.

The deposition system was arranged in a symmetric configuration with a rotating substrate holder for compositional uniformity. The base pressure of the sputtering chamber was typically $\sim 2\times 10^{-8}$ Torr, and substrates were inserted from a load lock into the main chamber to maintain a low base pressure. For the deposition of BIT thin films, an operating pressure of 10 mTorr was maintained during deposition. The total flow rates of Ar and O_2 gases were 10 sccm, as controlled by mass-flow controllers, for the stoichiometric thin films. The substrate temperature was fixed at about 600°C. The deposition time was usually 60 min. The film thickness was fixed at ~400nm.

The structural properties of the BIT thin films were characterized by XRD. Surface morphology was observed by SEM. Electrical properties were measured using the ferroelectric property measurement system RT-6000HVS. The polarization-electric field (*P-E*)

hysteresis loops were measured using one-shot triangular waveforms with a period of 50 ms. The dielectric constant (ε) was measured with LCR meter.

3. RESULTS AND DISCUSSION

Figure 1 (a) shows the effect of oxygen to argon ratio (OAR=Ar/(Ar+O_2)) of the composition ratio of BIT thin films on Pt/Ti/SiO_2/Si substrate. The RF powers of Bi_2O_3 and TiO_2 are fixed at 100 W and 200 W, which are determined by the result reported in ref.17. Oxygen partial pressure was changed by controlling flow rates of Oxygen and Argon into the sputtering chamber. The composition is Bi-rich and Ti-poor in OAR=0. At OAR increases, the compositions of Bi and Ti tend to move toward the two dashed lines. The stoichiometric composition is found in two points of OAR=0.6 and 1.0. These XRD patterns are shown in Fig. 1(b). Comparing each XRD pattern, the XRD pattern at OAR=0.6 is shown to be existence of the pyrochlore phase. The BIT thin film with *c*-axis orientation and single phase was obtained on OAR=1.0. However, large leakage current was ~5.0×10^{-4} A/cm^2. This is considered to be due to the oxygen vacancies of as-deposited BIT thin film. Thus, it is necessary to prevent the oxygen vacancies by other method.

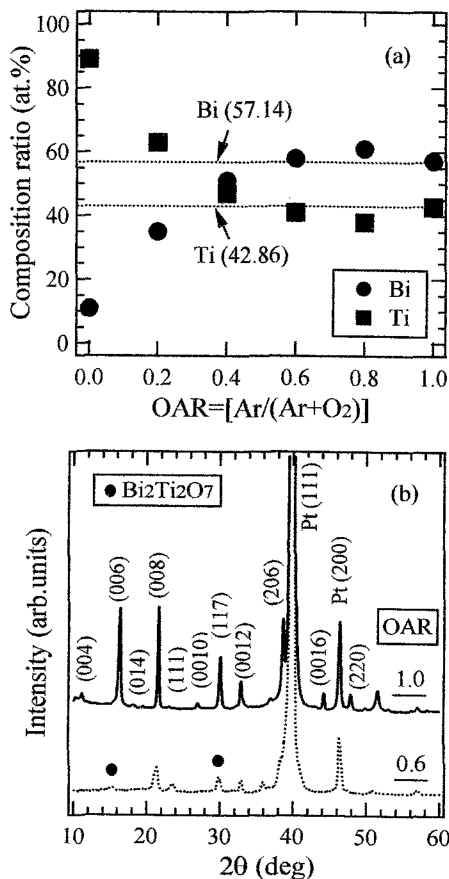

Fig. 1 (a) Composition ratio and (b) XRD pattern of Ar to O_2 ratio. The bottom axis is shown as OAR=[Ar/(Ar+O_2)].

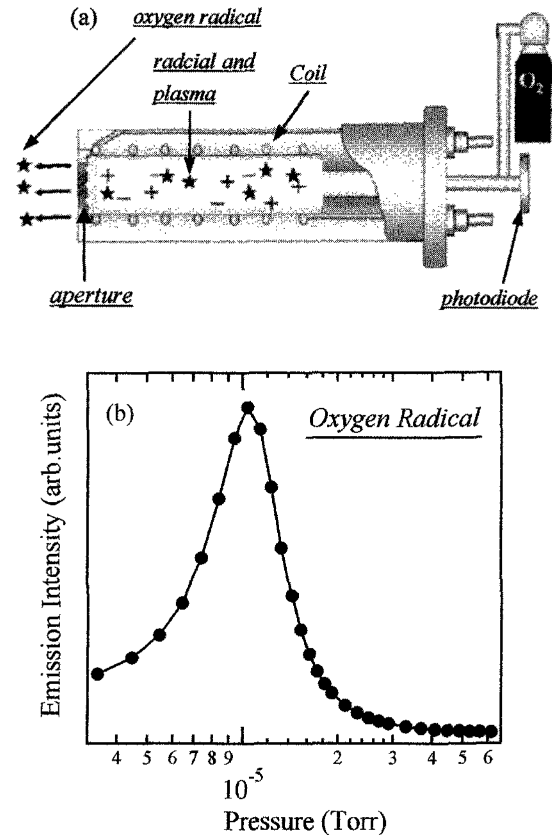

Fig. 2 (a) Schematic diagram of oxygen radical gun. (b) Emission intensity of oxygen radical as a function of vacuum pressure.

Figure 2(a) shows the schematic diagram of oxygen radical gun installed at sputtering system. The oxygen radical gun chamber consists of radio frequency coil, aperture, , and oxygen gas bomb. The oxygen radical is generated as follows. The oxygen gas supplied by gas bomb is introduced into the gun chamber. The RF power plays into the coil. Then, the plasma and radical are created in the radical gun. The oxygen radial is emitted into the sputtering chamber through the aperture. Therefore, the oxygen radical concentration depends on the vacuum pressure of the gun and RF power of coil.

Figure 2(b) shows the emission intensity of oxygen radical as a function of vacuum pressure in the radical gun. The emission intensity was measured using photodiode, as shown in Fig. 2(a). In this study, the RF power of the oxygen radical gun was fixed at 350 W. The emission intensity is in proportion to the oxygen radical concentration. The intensity increases with decreasing vacuum pressure. The maximum peak, which corresponds to the high radical concentration, is observed at 1.0×10^{-5} Torr.

Figure 3 shows the composition ratio as a function of distance between substrate and Bi_2O_3 target (S-T distance) in oxygen radical irradiated BIT thin films. The S-T distance of TiO_2 target was fixed at 80 mm. The authors have already reported that the deposition rate of Bi_2O_3 is higher than that of TiO_2 [17-21]. Therefore, the composition of oxygen radical irradiated BIT thin film is different from that of non-irradiated BIT thin film. When the S-T distance of Bi_2O_3 target is 100

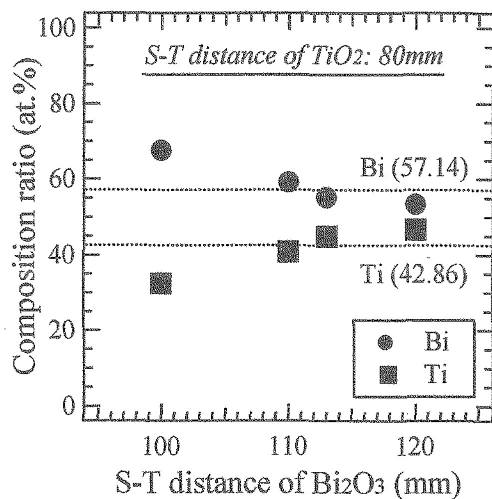

Fig. 3 Composition ratios of Bi and Ti as a function of distance of Bi_2O_3 target and substrate (S-T distance). The S-T distance of TiO_2 is fixed at 80 mm.

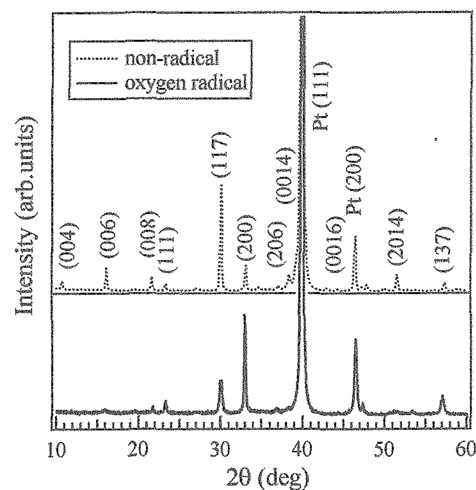

Fig. 4 XRD patterns of non-radical and oxygen-radical irradiated BIT thin films.

mm, the composition ratios of Bi and Ti markedly differ from the chemical stoichiometric composition, indicating that the deposition rate of Bi_2O_3 is significantly higher than that of TiO_2. The composition of Bi decreases with increasing S-T distance. The stoichiometric composition is found in S-T distance of 112 mm. On the other hand, the S-T distance of non-irradiated BIT thin film shown in Fig. 1 is 100 mm. The S-T distance of oxygen radical irradiated BIT thin film is longer than that of non-irradiated BIT thin film. This indicates that the reactive of Bi particle increases by the oxygen radical irradiation.

Figure 4 shows the XRD patterns of oxygen radical irradiated and non-irradiated BIT thin films. No evidence of Bi_2O_3 and pyrochlore phases is observed in these XRD patterns. The non-irradiated BIT thin film exhibits a highly *c*-axis orientation. The oxygen radical irradiated BIT thin film exhibits *a*- and *b*-axes orientation. The mechanism of *a*- and *b*-axes orientation of the oxygen radical irradiated BIT thin film is very complicated. The lattice mismatch between BIT and Pt substrate is estimated to be approximately 5.4 %. In general, the BIT thin film on Pt substrate exhibits *c*-axis orientation. Therefore, the concept of lattice mismatch cannot explain the *a*- and *b*-axes orientation of the oxygen radical irradiated BIT thin film.

In recent years, BIT thin films with a TiO_2 anatase buffer layer have been prepared on the $Pt/Ti/SiO_2/Si$ substrates by MOCVD [13,14]. The BIT thin film with the TiO_2 anatase buffer layer prepared at 500°C exhibited highly *a*- and *b*-axes-oriented BIT single phases, although the BIT thin film with no buffer layer exhibited a *c*-axis orientation. The ferroelectricity of the BIT thin film with the TiO_2 anatase buffer layer strongly depends on the thickness ratio of the BIT thin film to the TiO_2 anatase layer, indicating that the TiO_2 anatase buffer layer acts not as barrier layer but as an initial nucleation layer of the BIT thin film. However, the TiO_2 anatase layer was not used in this study.

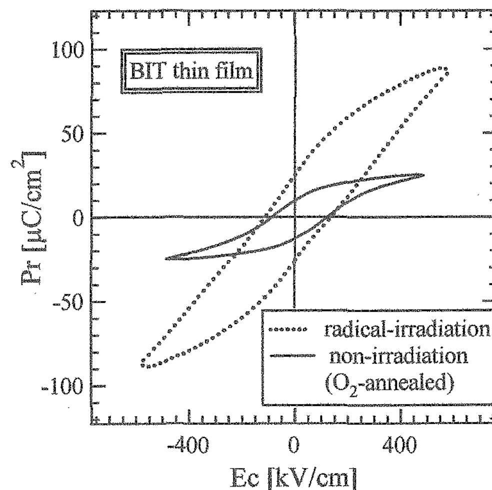

Fig. 5 Hysteresis loops of non-radical and oxygen-radical irradiated BIT thin films.

Figure 5 shows the hysteresis loops of non-irradiated and oxygen radical irradiated BIT thin films. The hysteresis loop of non-radical irradiated BIT thin film was not observed. This originates the oxygen vacancies of BIT thin film. Therefore, the non-irradiated BIT thin film was annealed at 800°C in an O_2 atmosphere for 1 h in order to investigate the effect of postannealing, although the oxygen radical irradiated BIT thin film was not annealed. The obtained hysteresis loops exhibit symmetrical shape. The P_r and E_c are $2P_r$=23.0 μC/cm^2 and $2E_c$=246 kV/cm, respectively. Then, the leakage current was ~10^{-4} A/cm^2. On the other hand, the oxygen radical irradiated BIT thin film exhibits hysteresis loop. The saturation of oxygen radical irradiated BIT thin film is lower than that of non-irradiated BIT thin film. Furthermore, the E_c and P_r are very large. However, the leakage current (~10^{-6} A/cm^2) is improved by oxygen radical irradiation when the voltage is 20 V.

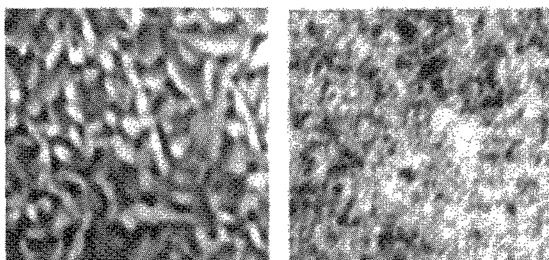

Fig. 6 SEM photographs of (a) non-radical and (b) oxygen-radical irradiated BIT thin films.

Figure 6 shows the SEM photographs of non-radical and oxygen radical irradiated BIT thin films. The non-radical BIT thin film consisted of well-developed grains with diameters of around 400 nm. The grain shape was isotopic and round. The large leakage current shown in Fig. 5 attributes the large grain size. The contribution of oxygen vacancies might also exist in the film. The oxygen radical irradiated BIT thin film consisted of small grains.

The *a*- and *b*-axes orientation, large E_c and small grain size of BIT thin film contribute to the effect of oxygen radical irradiation during the deposition. Similar phenomena have been observed in the BIT thin film with a TiO_2 anatase layer on Pt substrates prepared by MOCVD [13,14]. The ferroelectricity of the BIT thin film with the TiO_2 anatase layer strongly depends on the thickness ratio of the BIT thin film to the TiO_2 anatase layer. When the thickness of TiO_2 anatase layer is large, the saturation of hysteresis loop is very low since the TiO_2 anatase acts as low dielectric layer [14]. Although the interface between the BIT thin film and Pt substrate has not been clarified in this study, the TiO_2 layer created by oxygen radical with high reactive may exist in interface of the oxygen radical irradiated BIT thin film. Thus, to further investigate the mechanism of *a*- and *b*-axes orientation and ferroelectricity of oxygen radical irradiated BIT thin film, it is necessary to perform more systematic optimizations such as RF power of oxygen radical and substrate temperature during the deposition in the future study.

4. CONCLUSION

We have proposed novel process for the fabrication of BIT thin films by the two-dimensional RF magnetron sputtering with TiO_2 and Bi_2O_3 targets. In order to achieve low temperature crystallization, we tried to irradiate the oxygen radical with high reactive during the deposition. The oxygen radical irradiated BIT thin film exhibited *a*- and *b*-axes orientation, although the non-irradiated BIT thin film exhibited highly *c*-axis orientation. The prepared BIT thin film consisted of small grains. The BIT thin film exhibited the ferroelectricity without postannealing. These findings indicate that the oxygen radical irradiation is very effective for BIT thin film deposition.

ACKNOWLEDGEMENT

We would like to thank Mr. K. Kudoh and Mr. M. Takana for their technical support. This work was supported by a Grant-In- Aid for Scientific Research from the Ministry of Education, Culture, Sports, Science and Technology.

REFERENCES

[1] T. Kijima, M. Ushikubo and H. Matsunaga: Jpn. J. Appl. Phys. **38** (1999) 127.
[2] T. Kijima, S. Satoh, H. Matsunaga and M. Koba: Jpn. J. Appl. Phys. **35** (1996) 1246.
[3] T. Kijima and H. Matsunaga: Jpn. J. Appl. Phys. **37** (1998) 5171.
[4] T. Kijima and H. Matsunaga: Jpn. J. Appl. Phys. **38** (1999) 2281.
[5] T. Kijima, Y. Kawashima, Y. Idemoto and H. Ishiwara: Jpn. J. Appl. Phys. **41** (2002) L1164.
[6] S. Okamura, Y. Yagi, K. Mori, G. Fujihashi, S. Ando and T. Tsukamoto: Jpn. J. Appl. Phys. **36** (1997) 5889.
[7] M. Yamaguchi and T. Nagatomo: Thin Solid Films **348** (1999) 294.
[8] T. Watanabe and H. Funakubo: Jpn. J. Appl. Phys. **39** (2000) 5211.
[9] T. Watanabe, A. Saiki, K. Saito and H. Funakubo: J. Appl. Phys. **89** (2001) 3934.
[10] T. Watanabe, H. Funakubo, M. Osada, Y. Noguchi and M. Miyayama: Appl. Phys. Lett. **80** (2002) 100.
[11] M. Nakamura, T. Higuchi and T. Tsukamoto: Jpn. J. Appl. Phys. **42** (2003) 5687.
[12] M. Nakamura, T. Higuchi and T. Tsukamoto: Jpn. J. Appl. Phys. **42** (2003) 5969.
[13] M. Nakamura, T. Higuchi Y. Hachisu and T. Tsukamoto: Jpn. J. Appl. Phys. **43** (2004) 1449.
[14] T. Higuchi, M. Nakamura, Y. Hachisu, T. Hattori and T. Tsukamoto: Jpn. J. Appl. Phys. **43** (2004) 6585.
[15] Y. Masuda, H. Masumoto, A. Baba, T. Goto and T. Hirai: Jpn. J. Appl. Phys. **32** (1993) 4043.
[16] W. Jo, S. M. Cho, H. M. Lee, D. C. Kim and J. U. Bu: Jpn. J. Appl. Phys. **38** (1999) 2827.
[17] M. Tanaka, T. Higuchi, K. Kudoh and T. Tsukamoto: Jpn. J. Appl. Phys. **41** (2002) 1536.
[18] K. Kudoh, T. Higuchi, Y. Iwasa, M. Hosomizu and T. Tsukamoto: Proc. Inter. Symp. Appl. Ferro. (ISAF) **XIII** (2002) 167.
[19] T. Higuchi, M. Tanaka, K. Kudoh, T. Takeuchi, S. Shin and T. Tsukamoto: Jpn. J. Appl. Phys. **40** (2001) 5803.
[20] T. Higuchi, K. Kudoh, T. Takeuchi, Y. Masuda, Y. Harada, S. Shin and T. Tsukamoto: Jpn. J. Appl. Phys. **41** (2002) 7195.
[21] T. Higuchi, M. Iwasa, K. Kudoh and T. Tsukamoto: Trans. Mater. Res. Soc. Jpn. **29** (2004) 1121.

(Received December 10, 2005; Accepted January 31, 2006)